RSC Advances

PAPER

View Article Online
View Journal | View Issue

Cite this: *RSC Adv.*, 2024, **14**, 12142

Removal of diclofenac sodium from water using a polyacrylonitrile mixed-matrix membrane embedded with MOF-808†

Xiao-Jing Hu,[a] Yu-Lin Li,[b] Hai-Xiong Liu,[b] Shao-Ming Ying, *[a] Qi Yin *[b] and Tian-Fu Liu [b]

Received 20th December 2023
Accepted 1st April 2024

DOI: 10.1039/d3ra08682h

rsc.li/rsc-advances

MOF-808, owing to the synergistic effect of its large surface area and surface charge matching, showed a diclofenac sodium (DCF) removal capacity as high as 630 mg g^{-1}, and the ability to adsorb 436 mg g^{-1} DCF in two hours, outperforming many common Zr-MOFs under the same conditions. Importantly, a series of free-standing mixed-matrix membranes made by combining polyacrylonitrile with MOF-808 were fabricated and exhibited high efficiency of removing DCF from water *via* an easily accessible filtration method.

Owing to the escalating demand for human health and survival products, pharmaceuticals and personal care products (PPCPs) have been widely utilized, resulting in their ubiquitous presence in the natural environment.[1] However, most PPCPs resist complete biodegradation, posing a new and urgent challenge for their removal. Diclofenac sodium (DCF), one of the most commonly used PPCPs, is already detectable in surface water, causing potential risks to human health and the aquatic environment.[2]

Therefore, it is important and urgent to develop an efficient method for removing DCF from water, and numerous removal methods have been reported, such as adsorption, an advanced oxidation process, coagulation, and membrane processes. Using porous nanostructure materials as adsorbents is one of the most accessible and cost-effective methods for removing DCF from water. Thus, there is an urgent need to develop adsorbents with high DCF adsorption efficiency. Metal–organic frameworks (MOFs), a class of porous materials composed of organic linkers and inorganic nodes, have witnessed significant advances over the last few decades.[3] Thanks to their high crystallinity, diverse building blocks, and controllable pore shape/size, MOFs are useful in a variety of molecule separation and catalysis areas, as well as in biomedicine, sensor development, and PPCP removal applications.[4]

Membrane-based technologies offer an excellent alternative for removing pollutants, because of their advantage over powder nanoparticles in operation time, usability, and convenience. Traditional nanofiltration (NF) and reverse osmosis (RO) membranes show good separation performance in their rejecting almost all materials with particle sizes larger than the pore size, but difficulties in achieving selective molecule rejection. As a promising alternative, mixed-matrix membranes (MMMs) have garnered the interest of researchers for the ease in regulating their separation performance through the selection and modification of filler material and the superiority in the mass production of large-area membranes, which is important in industry applications.[5] For example, ZIF-8-based MMMs exhibit high selectivity and permeability for the C_3H_6/C_3H_8 pair.[6] Amino-functionalized ZIF-7-based MMMs are very attractive for applications such as natural-gas sweetening or biogas purification.[7] Otherwise, MMMs containing stable MOFs are also used for removing pollutants from water, because it is possible to improve the pollutant adsorption performance and selectivity of membrane adsorption by adjusting the pore size and structure of the MOFs. For instance, MMMs containing UiO-66-NH_2 show exceptional capabilities at adsorbing Cr^{VI} ions from water.[8] While several investigations have shown the potential applications of MOFs in DCF adsorption and of MMMs in pollutant removal, there have been few reports dedicated to preparing MOF-based MMMs for effective removal of DCF from water.

MOF-808, a well-known and accessible Zr-based MOF, has been used for DCF removal, due to its excellent framework stability.[9] Although the highly effective DCF adsorption performance of MOF-808 has been shown, useable MOF-based MMMs for removing DCF from water are not available. Herein, not only was proof provided for the remarkable DCF adsorption capacity of MOF-808, surpassing those of many typical Zr-MOFs

[a]*College of Chemistry and Materials, Fujian Provincial Key Laboratory of Featured Biochemical and Chemical Materials, Ningde Normal University, Ningde, Fujian 352100, P. R. China. E-mail: ysm@ndnu.edu.cn*

[b]*State Key Laboratory of Structural Chemistry, Fujian Institute of Research on the Structure of Matter, Chinese Academy of Sciences, Fuzhou, 350108, P. R. China. E-mail: yinqi@fjirsm.ac.cn*

† Electronic supplementary information (ESI) available. See DOI: https://doi.org/10.1039/d3ra08682h

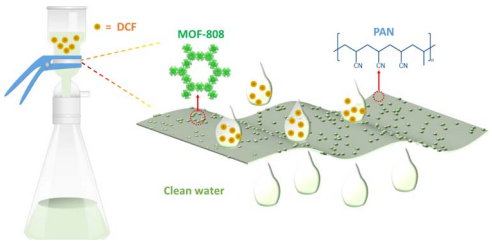

Scheme 1 Schematic diagram of the process involving the adsorption of DCF by MOF-808-based MMMs *via* an easily accessible filtration method.

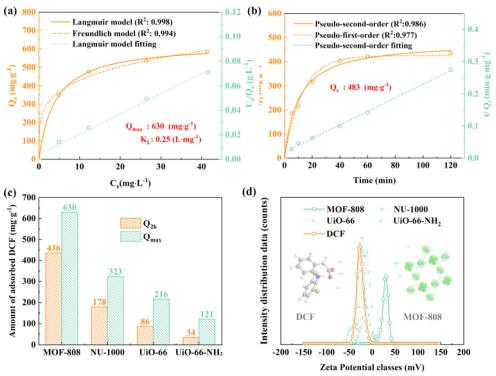

Fig. 1 (a) and (b) DCF adsorption isotherms and kinetics of MOF-808. (c) DCF adsorption capacities of indicated MOFs. (d) Zeta potential results for DCF and indicated MOFs.

including NU-1000, UiO-66, and UiO-66-NH_2, under the same experimental conditions, but the synergistic effect of high surface area and strong electrostatic attraction between DCF and MOF-808 was also tested and confirmed. Importantly, a series of MOF-based MMMs containing different MOF-808 loadings was prepared through an easy casting method; also a facile filtration for removing DCF from the aqueous solutions was exploited (Scheme 1).

We first prepared powdery MOF-808, whose purity was confirmed according to the good consistency between experimental powder X-ray diffraction (PXRD) and simulated patterns (Fig. S1†). Its BET surface area (1991 $m^2\ g^{-1}$) was calculated from N_2 sorption isotherms at 77 K and matched those previously reported (Fig. S4†).[10] The scanning electron microscopy (SEM) image acquired of MOF-808 particles displayed a clear regular octahedral morphology (Fig. S5†), and corresponding size distribution analysis showed dimensions of the MOF-808 particles ranging from 80 nm to 200 nm, with a D (50) value equals to 136 nm (Fig. S6†). Furthermore, PXRD patterns confirmed that MOF-808 can maintain its crystallinity after being soaked for 24 h in various aqueous solutions with pH values from 1 to 12 (Fig. S7†). In summary, we successfully prepared nano-sized MOF-808 with high porosity and excellent stability, having the potential to adsorb DCF from aqueous solutions.

To evaluate the DCF adsorption performance of MOF-808, an adsorption isotherm study was performed first. Both Langmuir and Freundlich models, as shown in Fig. 1a, were used to describe the adsorption behaviour; the relevant mathematical expressions and fitting results are given in eqn (S1) and (S2) and Table S1.† As can be seen from the results, the R^2 of the Langmuir model (0.998) was slighter higher than that of the Freundlich model (0.994), indicative of the Langmuir model fitting better the behaviour of monolayer adsorption. According to the Langmuir model, the maximum adsorption capacity (Q_{max}) was 630 mg g^{-1}, superior to those of most reported Zr-based MOFs, Cu-based MOFs, Fe-based MOFs, and Al-based MOFs, each with a Q_{max} value under 600 mg g^{-1} (Table S2†).[11,12] Also, the adsorption capacity of MOF-808 at a low DCF concentration (1 mg L^{-1}) was determined according to the Langmuir isotherm slope ($Q_{max} \times K_L = 157$ L g^{-1}) to be 157 mg g^{-1}, better than those of most MOFs and activated carbon materials.[12] In short, the adsorption isotherm confirmed the high DCF adsorption capacity and affinity of MOF-808.

In addition, the dependence of the DCF adsorption performance of MOF-808 on time was also examined (Fig. 1b). Rapid adsorption occurred in the initial forty minutes, and about 84.2% ($Q_t = 421$ mg g^{-1}) of the DCF was removed in the first hour, and the final adsorption capacity, *i.e.*, at two hours, reached 436 mg g^{-1}. To characterize the adsorption behaviour of MOF-808, pseudo-first-order and pseudo-second-order models were tested to characterize the kinetics of adsorption process (Fig. 1b); the relevant mathematical expressions and corresponding kinetics parameters are presented in eqn (S3) and (S4) and Table S3.† The correlation coefficient (R^2) of the pseudo-second-order kinetics model (0.986) was higher than that of the pseudo-first-order model (0.977), indicative of the pseudo-second-order model fitting the data better, and indicative of the presence of specific interactions between MOF-808 and DCF. Based on this model, the DCF adsorption capacity at equilibrium (Q_e) was predicted to be 483 mg g^{-1}, close to the experimental results (Q_{2h}), indicative of chemisorption being the main interaction in the adsorption process.

To further appraise the DCF adsorption performance of MOF-808, another three zirconium-based MOFs, namely UiO-66, UiO-66-NH_2 and NU-1000, were also investigated. As seen in Fig. 1c, UiO-66 and UiO-66-NH_2 showed much lower DCF adsorption capacities than did MOF-808 in two hours. Considering the higher surface area of MOF-808 than those of UiO-66 and UiO-66-NH_2 (MOF-808: 1991 $m^2\ g^{-1}$; UiO-66: 1110 $m^2\ g^{-1}$; UiO-66-NH_2: 1112 $m^2\ g^{-1}$),[13] we supposed that achieving a high surface area can be conducive to improving DCF adsorption performance. As for NU-1000 with its large surface area (2320 $m^2\ g^{-1}$),[14] though exhibiting much higher DCF adsorption capacity than UiO-66 and UiO-66-NH_2, its performance was also poorer than that of MOF-808. Meanwhile, the adsorption isotherms of the three MOFs also confirmed the difference between their DCF adsorption capacities and that of MOF-808. As shown in Fig. S12 and Table S4,† the adsorption behaviours of the three MOFs were also fitted well by the Langmuir model. Also, their calculated Q_{max} values were 323 mg g^{-1} for NU-1000, 216 mg g^{-1} for UiO-66 and 121 mg g^{-1} for UiO-66-NH_2, all lower than the value of MOF-808.

The above results showed that, apart from high surface area, there could be another factor impacting the DCF removal performance of MOFs. Considering that DCF can become partially dissociated in aqueous solution, forming the negatively charged anion DCF^- and positively charged Na^+ and considering that different MOFs have distinctive charges, we inferred that electrostatic attraction between DCF^- and MOFs is the critical factor accounting for its high DCF removal performance. To validate this hypothesis, zeta potential measurements of MOFs and DCF were taken. The results (Fig. 1d) indicated MOF-808 to be significantly positively charged, while DCF and other MOFs to be negatively charged. Thus, the charge matching would make for stronger electrostatic attraction between the negatively charged DCF and positively charged MOF-808 than that between DCF and other negatively charged MOFs, resulting in a higher DCF adsorption capacity. Thus, a synergistic effect of large surface area and surface charge matching was concluded to endow MOF-808 with high DCF adsorption performance.

Inspired by the excellent DCF adsorption performance of MOF-808, a series of free-standing MMMs, with different mass ratios of MOF-808 to PAN, were fabricated, done so by casting the solution containing MOF-808 particles and polymers onto a smooth glass plate. The details of the preparation procedure are shown in ESI.† The obtained membranes are denoted as M-*X* (M: membrane, *X*: mass percentage of the composite of MOF-808 and PAN made up of MOF-808). We prepared five different membranes, as shown in Fig. S13,† including pure PAN membrane, M-20%, M-40%, M-60%, and M′-60%, to investigate the DCF removal capacities of MOF-808-based MMMs.

First, the presence of MOF-808 in the obtained membranes was clarified and analysed using PXRD (Fig. 2a). All the MMMs yielded PXRD patterns matching that of MOF-808, and the intensities of the PXRD signals grew as the MOF-808 content was increased from 20% to 60%, indicating the presence of MOF-808 particles in the membranes and the increasing MOF-808 content from 20% to 60%. In contrast, the pure PAN membrane did not show crystallinity. These results revealed that MOF-808-based MMMs were prepared successfully. The surface and cross-sectional morphologies of the membranes were characterized using SEM. As shown in Fig. 2b–e, S14 and S15,† the surfaces of all the MMMs were similar to that of the pure PAN membrane, but there were homogeneous distributions of MOF-808 at the surfaces of the MMMs, according to the EDS mappings. Moreover, each of the membranes showed a loose and porous structure, with a thickness of ~10 μm for each of M-20%, M-40% and M-60%, and ~7 μm for M′-60%, all favourable for removing DCF from aqueous solution. Besides, neither cracks nor deformations were observed in the membrane surface after subjecting the membrane to a bending operation, taking M-60% as an example, which confirmed the toughness of the MMMs (Fig. S16†).

Following the successful preparation of MOF-808-based MMMs, we further evaluated the DCF extraction ability of these membranes by using an accessible vacuum filter device (Fig. S17†). Herein, the DCF removal efficiency (RE), calculated from the difference between DCF concentration before and after

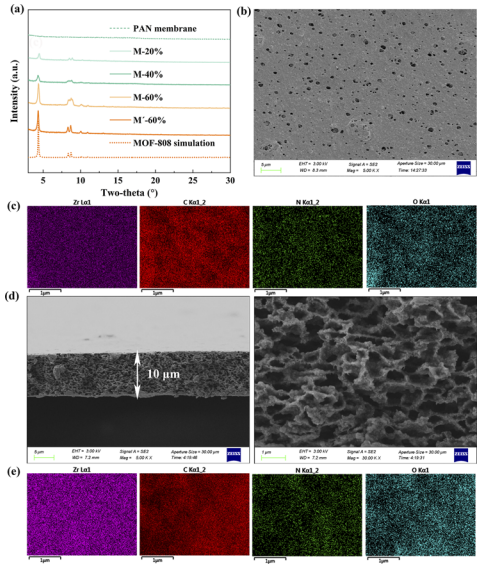

Fig. 2 (a) PXRD patterns of the prepared membranes. (b) Surface morphology of M-60%. (c) EDS mappings of the surface of M-60%. (d) Cross-sectional view of M-60%. (e) EDS mappings of the cross-sectional structure of M-60%.

five filtrations, was employed to evaluate the performances of the MMMs; see corresponding detailed equation in eqn (S5).† As seen in Fig. 3a, M-PAN could not remove DCF from an aqueous solution even after filtering five times. On the other hand, all the MMMs exhibited a distinct removal of DCF from the first to fifth filtration (Fig. S18†), with an increasing removal capacity as the MOF-808 content was increased from 20% to 60%. Note that M-60% could remove 91% of the DCF from an aqueous solution, the most of any of the MMMs, attributed to it having the highest MOF-808 content. In addition, membrane thickness also influenced the efficiency of removing DCF. As depicted in Fig. 3b, M′-60%, with a thinner membrane, exhibited poorer DCF removal capacity than did M-60%, probably due to the presence of fewer MOF-808 particles in the thinner membrane, which apparently adsorbed fewer DCF

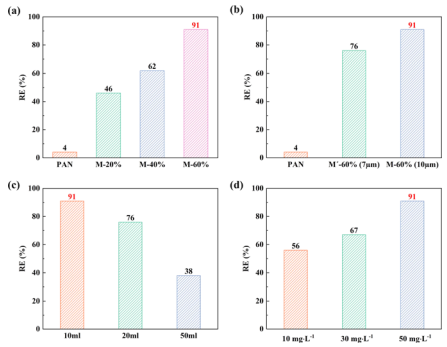

Fig. 3 (a) Removal efficiency levels of indicated membranes. (b) Removal efficiency levels of M-60% with indicated thicknesses. (c) Removal efficiency levels of M-60% for indicated volumes of the DCF solution. (d) Removal efficiency levels of M-60% for indicated DCF concentrations.

molecules and hence displayed a poorer performance. The performances of M-60% for DCF with different volumes and concentrations were also tested. As shown in Fig. 3c, M-60% could remove 76% and 38% of the DCF when the solution volumes were 20 mL, and 50 mL, respectively. Besides, M-60% could only remove 67% and 56% of the DCF when the concentrations of DCF in the solution were, respectively, 30 mg L^{-1} and 10 mg L^{-1} (Fig. 3d). Several plausible reasons for these results could be put forth, including low affinity of adsorbent and low strength of adsorption of diclofenac on the MOF-808 pores, according to previous reports.[12,15] In summary, the obtained MOF-808-based MMMs can remove DCF from an aqueous solution *via* an easily accessible filtration method, and the capacity of MMM to remove DCF could be adjusted by changing the MOF content and membrane thickness, and be influenced by aqueous volume and DCF concentration.

To study the adsorption mechanism of the MMMs, the pore sizes of the obtained membranes were investigated. As shown in Fig. S22,† the pores of all the membranes had dimensions greater than 100 nm, much larger than DCF (0.96 × 0.708 × 0.472 nm), and hence excluding the effect of membrane rejection and confirming the adsorption of MOF-808, corresponding to the experimental vacuum filtration results. In addition, adsorption isotherms of M-60% were acquired and its adsorption kinetics was analyzed. As shown in Fig. 4a and Tables S5 and S6,† the Langmuir model fitted these data better than did the Freundlich model (R^2: 0.999 > 0.980), indicative of similar adsorption behaviours for M-60% and pure MOF-808; and the Q_{max} was 222 mg g^{-1}, comparable to that activated carbon.[12] However, the adsorption kinetics of M-60% was slightly better with the pseudo-first-order model than with the pseudo-second-order model (R^2: 0.989 > 0.983). This result was indicative of a distinct adsorption process that could be attributed to the different diffusion paths of MMMs and pure MOF-808, with DCF taking more time to reach MOF-808 of MMMs, and leading to the lower adsorption capacity of MMMs at the same condition.

In conclusion, our study has revealed an outperforming DCF adsorption capability of MOF-808 through a comparison of MOF-808 with three other zirconium-based MOFs (NU-1000, UiO-66, and UiO-66-NH_2). The high performance can be ascribed to the synergistic effect of high surface area and surface charge matching between MOF-808 and DCF in the adsorption process. We successfully fabricated a series of free-standing MOF-based MMMs through a straightforward casting method and determined their abilities to remove DCF from aqueous solutions using an accessible vacuum filtration technique. The findings and efficient approach in this work offer a significant advance in the field of water purification, addressing the urgent need for effective methods to remove pharmaceutical pollutants from our water sources.

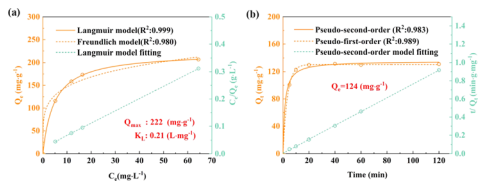

Fig. 4 (a) DCF adsorption isotherm of M-60%. (b) DCF adsorption kinetics of M-60%.

Author contributions

Xiao-Jing Hu: experimental operation, data curation, formal analysis, methodology, writing – original draft. Shao-Ming Ying: funding acquisition, supervision, writing – review & editing. Qi Yin: formal analysis, writing – review & editing. Yu-Lin Li: visualization, software, data curation. Hai-Xiong Liu: data curation, resources. Tian-Fu Liu: methodology, resources.

Conflicts of interest

There are no conflicts to declare.

Acknowledgements

We acknowledge financial support from the Natural Science Foundations of Fujian Province of China (Grant No. 2021J05252, 2022J011209), the Project of Scientific Research of Ningde Normal University (Grant No. 2020Y015), and the Innovation Team Project of Ningde Normal University (Grant No. 2021T07).

Notes and references

1 (*a*) J. Tong, L. Chen, J. Cao, Z. Yang, W. Xiong, M. Jia, Y. Xiang and H. Peng, *Sep. Purif. Technol.*, 2022, **294**, 121064; (*b*) C.-Y. Wang, C.-C. Wang, X.-W. Zhang, X.-Y. Ren, B. Yu, P. Wang, Z.-X. Zhao and H. Fu, *Chin. Chem. Lett.*, 2022, **33**, 1353–1357; (*c*) J. Zhong, X. Yuan, J. Xiong, X. Wu and W. Lou, *Environ. Res.*, 2023, **226**, 115633.

2 (*a*) Z. Hasan, N. A. Khan and S. H. Jhung, *Chem. Eng. J.*, 2016, **284**, 1406–1413; (*b*) S. Rojas and P. Horcajada, *Chem. Rev.*, 2020, **120**, 8378–8415.

3 L. Jiao, Y. Wang, H.-L. Jiang and Q. Xu, *Adv. Mater.*, 2018, **30**, e1703663.

4 (*a*) R.-B. Lin, S. Xiang, H. Xing, W. Zhou and B. Chen, *Coord. Chem. Rev.*, 2019, **378**, 87–103; (*b*) Z. Hu, B. J. Deibert and J. Li, *Chem. Soc. Rev.*, 2014, **43**, 5815–5840; (*c*) Z.-B. Fang, T.-T. Liu, J. Liu, S. Jin, X.-P. Wu, X.-Q. Gong, K. Wang, Q. Yin, T.-F. Liu, R. Cao and H.-C. Zhou, *J. Am. Chem. Soc.*, 2020, **142**, 12515–12523; (*d*) J. Sun, X. Zhang, D. Zhang, Y.-P. Chen, F. Wang, L. Li, T.-F. Liu, H. Yang, J. Song and R. Cao, *CCS Chem.*, 2022, **4**, 996–1006.

5 (*a*) L. Wang, X. Feng, L. Ren, Q. Piao, J. Zhong, Y. Wang, H. Li, Y. Chen and B. Wang, *J. Am. Chem. Soc.*, 2015, **137**, 4920–4923; (*b*) Y. Lu, H. Zhang, J. Y. Chan, R. Ou, H. Zhu, M. Forsyth, E. M. Marijanovic, C. M. Doherty, P. J. Marriott, M. M. B. Holl and H. Wang, *Angew. Chem., Int. Ed.*, 2019, **58**, 2–10; (*c*) X. Chen, D. Chen, N. Li, Q. Xu, H. Li, J. He and J. Lu, *ACS Appl. Mater. Interfaces*, 2020, **12**, 39227–39235.

6 D. Liu, L. Xiang, H. Chang, K. Chen, C. Wang, Y. Pan, Y. Li and Z. Jiang, *Chem. Eng. Sci.*, 2019, **204**, 151–160.
7 L. Xiang, L. Sheng, C. Wang, L. Zhang, Y. Pan and Y. Li, *Adv. Mater.*, 2017, **29**, 1606999.
8 Y. Zhang, X. Feng, H. Li, Y. Chen, J. Zhao, S. Wang, L. Wang and W. Bo, *Angew. Chem., Int. Ed.*, 2015, **54**, 4259–4263.
9 N. Prasetya and K. Li, *Chem. Eng. J.*, 2021, **417**, 129216.
10 H. Furukawa, F. Gándara, Y.-B. Zhang, J. Jiang, W. L. Queen, M. R. Hudson and O. M. Yaghi, *J. Am. Chem. Soc.*, 2014, **136**, 4369–4381.
11 S. Zhuang, R. Cheng and J. Wang, *Chem. Eng. J.*, 2019, **359**, 354–362.
12 N. Prasetya, I. G. Wenten, M. Franzreb and C. Wöll, *Coord. Chem. Rev.*, 2023, **475**, 214877.
13 S. J. Garibay and S. M. Cohe, *Chem. Commun.*, 2010, **46**, 7700–7702.
14 P. Deria, J. E. Mondloch, E. Tylianakis, P. Ghosh, W. Bury, R. Q. Snurr, J. T. Hupp and O. K. Farha, *J. Am. Chem. Soc.*, 2013, **135**, 16801–16804.
15 M. D. G. de Luna, Murniati, W. Budianta, K. K. P. Rivera and R. O. Arazo, *J. Environ. Chem. Eng.*, 2017, **5**, 1465–1474.